# Identification of Large-Scale Atmospheric and Oceanic Features from *IRS-P4* Multifrequency Scanning Microwave Radiometer: Preliminary Results

RASHMI SHARMA, K. N. BABU, A. K. MATHUR, AND M. M. ALI

*Oceanic Sciences Division, Meteorology and Oceanography Group, Space Applications Centre, Ahmedabad, India*

20 July 2001 and 12 December 2001

ABSTRACT

Large-scale features of sea surface temperature, wind speed, water vapor, and cloud liquid water, derived from multifrequency scanning microwave radiometer (MSMR) on board Indian oceanographic satellite *IRS-P4* could be identified during 15 June–23 August 1999. This is the period during which extensive validation was carried out. MSMR is the only sensor in orbit operating at 6.6 GHz. Average distribution of these parameters brings out large-scale atmospheric and oceanographic features. Zonal averages of these parameters were also studied to examine the consistency of MSMR data over larger spatial scales. Linear correlations between all parameters were also computed to check for the interconsistency of these parameters. The present analysis shows the potential use of MSMR products in studying the oceanographic and atmospheric phenomena.

## 1. Introduction

The Indian Space Research Organisation (ISRO) launched *Oceansat-I* on 26 May 1999. This is also known as Indian Remote Sensing Satellite *IRS-P4* and carries two oceanographic payloads, an ocean color monitor (OCM) and a multifrequency scanning microwave radiometer (MSMR). While the OCM measures the oceanographic parameters in eight spectral bands ranging from 402–885 nm, MSMR measures the emitted radiation in four microwave frequencies with dual polarizations. The specifications of MSMR are given in Table 1. MSMR is the only sensor in orbit operating at 6.6 GHz.

The orbital characteristics of the *IRS-P4* satellite result in almost global coverage, with a repeat cycle of 2 days. However, 80% of the entire globe is covered on any single day. The four geophysical parameters available from MSMR are sea surface temperature (SST), wind speed (WS), integrated water vapor (WV), and cloud liquid water (CLW) content. Gohil et al. (2000) derived the geophysical parameters through simulations using a radiative transfer model.

Microwave radiometers viewing the sea surface from space observe the thermal radiation emitted by the surface and by the atmosphere as well as the radiation reflected by the sea surface in the microwave part of the electromagnetic spectrum. Microwave sensors are capable of operating under all weather conditions, as the atmospheric absorption and scattering are practically absent at these longer wavelengths. Hence, a continuous time series of data can be obtained for oceanic and atmospheric applications irrespective of the cloud cover, which otherwise is the limitation of infrared (IR) sensors. However, the disadvantage of the microwave radiometers is the poor spatial resolutions compared to visible and IR sensors, due to the present limitation on antenna size and weak emission from the ocean and atmosphere at these higher wavelengths. Despite this limitation, microwave radiometers have become useful components in the remote sensing observation systems. Earlier radiometers flown on board *Seasat* and the Nimbus satellites, and present ones on Defense Meteorological Satellite Program (DMSP) and Tropical Rainfall Measuring Mission (TRMM) spacecrafts demonstrated their usefulness in the areas of oceanic, atmospheric, sea ice, and land studies. Bernstein (1982) and Bernstein and Morris (1983), using *Seasat* Scanning Mutichannel Microwave Radiometer (SMMR) data, mapped the SST distribution of the tropical and midlatitude North Pacific. They suggested that the regular and uniform coverage of a single sensor, despite its inherent inaccuracy of ~1°C, is able to produce a better map than irregular sampling from ships. Wentz et al. (2000) have demonstrated the possible use of TRMM Microwave Imager (TMI) derived SST in studies related to tropical instability waves, marine boundary layer dynamics, and the

*Corresponding author address:* Dr. M. M. Ali, Oceanography Group, National Remote Sensing Agency, Hyderabad 500 037, India. E-mail: mmali73@yahoo.com

TABLE 1. Specifications of MSMR.

| | | | | |
|---|---|---|---|---|
| Frequency (GHz) | 6.6 | 10.65 | 18.0 | 21.0 |
| Spatial resolution (km) | 105 × 68 | 66 × 43 | 40 × 26 | 34 × 22 |
| Polarization | Vertical and horizontal | | | |
| Swath | 1360 km for all frequencies | | | |
| Nominal incidence angle | 49.7° | | | |
| Radiometer sensitivity | Better than 1 K | | | |
| Dynamic range | 10–330 K | | | |
| Data rate | 6.4 kb $s^{-1}$ | | | |

prediction of hurricane intensity. Chelton et al. (1981) demonstrated the possible contribution of SMMR (onboard *Seasat* spacecraft) derived WV data to climate research. Satellite measurement of WV is a useful source of additional humidity information in analysis over the ocean, where conventional measurements (radiosonde data, meteorological data, etc.) are very sparse. Yang and Smith (1999) suggested the possibility of using a Special Sensor Microwave Imager (SSM/I) along with large-scale sounding data to retrieve latent heat for studying the role of cumulus convection on diabatic heating over tropical oceans. The distribution of the total WV content for the entire Northern Hemisphere was carried out by Starr and White (1955) and Starr and Peixoto (1958), among others. A more complete study of global distribution of total WV content was carried out by Starr et al. (1969).

In this paper, preliminary results of the global analyses of SST, WS, WV, and CLW, derived from MSMR onboard *IRS-P4* were presented for the first 70 days (15 June–23 August 1999) of the observations, during which extensive validation was carried out. The major objective was to deduce the large-scale features of these parameters. For this purpose, both monthly mean and zonal averages were analyzed.

## 2. Retrieval algorithm

Though the objective of the present paper is to use the MSMR-derived Geophysical Parameter Data (GPD) to study the large-scale oceanographic and atmospheric features, a brief summary of the retrieval algorithm used by Gohil et al. (2000) to derive the GPDs is given below.

The general form of the algorithm for the retrieval of a GPD (SST, WS, WV, or CLW), $G$, is

$$G = C_0(\mathrm{CSST}, \theta) + \sum_{i=1}^{i=N} C_i(\mathrm{CSST}, \theta) \cdot f[\mathrm{TB}_i(M, R, \theta)],$$

where *CSST*, the season- and region-specific monthly mean climatic SST, is a function of brightness temperature specific to the month, $M$, and geophysical location, $R$, of MSMR; $C_0$ and $C_i$ are the retrieval coefficients for the $i$th channel, $\mathrm{TB}_i$ is the brightness temperature of the $i$th channel, $N$ is the total number of channels used, and $f$ is the function of brightness temperature. This function is linear for 6.6- and 10.6-GHz frequencies, while it is logarithmic for the other two frequencies.

Thus the retrieval models for SST, WS, WV, and CLW are given by

$$\begin{aligned}
\mathrm{SST} &= t_0 + t_1\mathrm{TB6V} + t_2\mathrm{TB6H} + t_3\mathrm{TB10V} \\
&\quad + t_4\mathrm{TB10H} + t_5 \ln(280 - \mathrm{TB18V}) \\
&\quad + t_6 \ln(280 - \mathrm{TB18H}) + t_7 \ln(280 - \mathrm{TB21V}) \\
&\quad + t_8 \ln(280 - \mathrm{TB21V}) \\
\mathrm{SW8} &= p_0 + p_1\mathrm{TB6V} + p_2\mathrm{TB6H} + p_3\mathrm{TB10V} \\
&\quad + p_4\mathrm{TB10H} + p_5 \ln(280 - \mathrm{TB18V}) \\
&\quad + p_6 \ln(280 - \mathrm{TB18H}) \\
&\quad + p_7 \ln(280 - \mathrm{TB21V}) + p_8 \ln(280 - \mathrm{TB21H}) \\
\mathrm{SW6} &= q_0 + q_1\mathrm{TB10V} + q_2\mathrm{TB10H} \\
&\quad + q_3 \ln(280 - \mathrm{TB18V}) \\
&\quad + q_4 \ln(280 - \mathrm{TB18H}) + q_5 \ln(280 - \mathrm{TB21V}) \\
&\quad + q_6 \ln(280 - \mathrm{TB21H}) \\
\mathrm{WV} &= v_0 + v_1 \ln(280 - \mathrm{TB18V}) \\
&\quad + v_2 \ln(280 - \mathrm{TB18H}) + v_3 \ln(280 - \mathrm{TB21V}) \\
&\quad + v_4 \ln(280 - \mathrm{TB21H}) \\
\mathrm{LWC} &= c_0 + c_1 \ln(280 - \mathrm{TB18V}) + c_2 \ln(280 - 18\mathrm{H}) \\
&\quad + c_3 \ln(280 - 21\mathrm{V}) + c_4 \ln(280 - 21\mathrm{H})
\end{aligned}$$

where $t_i$, $p_i$, $q_i$, $v_i$, and $c_i$ are climate SST and incident angle–dependent retrieval coefficients. LWC is liquid water content. SW8 is the WS using all the channels, and SW6 is that using six channels, that is, without using 6.6 GHz (both vertical and horizontal). These coefficients were derived using simulated brightness temperatures, through a radiative transfer model, and simulated environmental parameters. The brightness temperature (TB) simulations using the radiative transfer model involved computation of (i) atmospheric absorption (Liebe 1985) for the given frequency and incidence angle of MSMR for the known atmospheric constituents like dominant gases and hydrometeors and (ii) ocean surface emissivity (Hollinger 1971; Stogym 1972) for the given frequency, incidence angle, and the polarization of the MSMR for the known ocean surface physical conditions, like SST, salinity, winds, and foam (Wilheit 1979). Channels are 6.6 GHz horizontal (6H), and vertical (6V), etc. (Table 2).

Simulation of brightness temperatures in turn needs the vertical atmospheric profiles of temperature, pressure, humidity, and CLW density. Temperature profiles were simulated using lapse rates prevailing over global

TABLE 2. MSMR products and grid sizes.

| Product | Frequencies used [vertical and horizontal (V) and (H)] | Grid size (km) | Grid type |
|---|---|---|---|
| SST | 6.6, 10.65, 18.0, 21.0 | 150 × 150 | Grid I |
| WS | 6.6, 10.65, 18.0, 21.0 | 150 × 150 | Grid I |
| WS | 10.65, 18.0, 21.0 | 75 × 75 | Grid II |
| WV | 18.0, 21.0 | 50 × 50 | Grid III |
| CLW | 18.0, 21.0 | 50 × 50 | Grid III |

oceans. The pressure profiles were computed from the hydrostatic equation using the normal values at the surface. The relative humidity from the surface to the top of the atmosphere was estimated as a linear function, depending upon the SST of the region. CLW content profiles were estimated by introducing clouds of varying thickness at different altitudes and by assuming that CLW density diminishes from freezing level to the boundaries of clouds. These simulations were carried out for tropical, midlatitude, and polar regions separately.

Before retrieving the GPD, the TB values were checked for their quality. For the following reasons some TB values were rejected: (i) lying within 200 km of the coast (to avoid land contamination), (ii) the vertical polarized value for any channel being less than the horizontal polarized value, and (iii) the high-frequency values being less than the low-frequency values, irrespective of the polarization. Also, the TB values lying outside the range 10–279 K were not considered. The data are flagged as bad if the CLW and WV are more than 80 mg $cm^{-2}$ and 8 g $cm^{-2}$, respectively. These thresholds were set depending upon the simulation studies.

## 3. The GPDs

The GPDs are available in three different grid sizes of 150 km × 150 km (grid I), 75 km × 75 km (grid II), and 50 km × 50 km (grid III). The frequencies used in deriving these products and the grid sizes are summarized in Table 2. Water vapor and CLW are also available as grid I and grid II products. Thus, SST is available only for the 150 km × 150 km resolution, and WS at two resolutions of 150 km × 150 km and 75 km × 75 km, whereas WV and CLW are available for all the three cell sizes of 150 km × 150 km, 75 km × 75 km, and 50 km × 50 km.

TABLE 3. Comparison of MSMR products with in situ observations.

| Parameter | No. of points | Rmsd | Bias | Rmsd (after bias removal) |
|---|---|---|---|---|
| SST | 153 | 1.49 K | 0.98 K | 1.13 K |
| WS | 162 | 2.42 m $s^{-1}$ | 1.62 m $s^{-1}$ | 1.80 m $s^{-1}$ |
| WV | 16 | 0.53 g $cm^{-2}$ | 0.39 g $cm^{-2}$ | 0.32 g $cm^{-2}$ |

TABLE 4. Comparison of MSMR WS (m $s^{-1}$) with TMI and SSM/I observations.

| Grid | Time | No. of points | Rmsd | Bias | Rmsd (after bias removal) |
|---|---|---|---|---|---|
| | | TMI vs MSMR | | | |
| | < 1 h | 24 953 | 2.93 | −1.81 | 2.31 |
| 75 km | < 2 h | 40 321 | 2.95 | −1.85 | 2.29 |
| | < 3 h | 54 246 | 2.97 | −1.87 | 2.31 |
| | < 1 h | 10 254 | 2.68 | −1.78 | 2.01 |
| 150 km | < 2 h | 16 570 | 2.70 | −1.82 | 1.99 |
| | < 3 h | 22 196 | 2.72 | −1.84 | 2.00 |
| | | SSM/I F14 vs MSMR | | | |
| 75 km | < 2 h | 9131 | 3.01 | −1.01 | 2.84 |
| | < 3 h | 66 354 | 2.88 | −1.41 | 2.51 |
| 150 km | < 2 h | 3342 | 2.63 | −1.07 | 2.40 |
| | < 3 h | 25 658 | 2.69 | −1.57 | 2.18 |

## 4. The validation of GPDs

Ali et al. (2000) validated the MSMR-derived SST, WS, and WV observations during 15 June–23 August 1999 with the in situ observations over the Indian Ocean. The biases and the root-mean-square differences (rmsd) before/after removing the biases obtained by them are summarized in Table 3. They could not validate the CLW, as in situ measurements were not available. However, they could validate with other satellite products.

Wentz et al. (2000) compared TMI-derived SST with ocean buoys and found an rmsd of the order of 0.6°C,

TABLE 5. Comparison of MSMR WV (g $cm^{-2}$) with TMI and SSM/I observations.

| Grid | Time | No. of points | Rmsd | Bias | Rmsd (after bias removal) |
|---|---|---|---|---|---|
| | | TMI vs MSMR | | | |
| | < 1 h | 27 543 | 0.46 | −0.23 | 0.40 |
| 50 km | < 2 h | 44 692 | 0.46 | −0.22 | 0.40 |
| | < 3 h | 60 859 | 0.45 | −0.20 | 0.40 |
| | < 1 h | 26 626 | 0.46 | −0.22 | 0.40 |
| 75 km | < 2 h | 43 238 | 0.46 | −0.22 | 0.40 |
| | < 3 h | 58 898 | 0.46 | −0.20 | 0.41 |
| | < 1 h | 10 884 | 0.43 | −0.21 | 0.37 |
| 150 km | < 2 h | 17 673 | 0.43 | −0.21 | 0.38 |
| | < 3 h | 23 953 | 0.53 | −0.19 | 0.38 |
| | | SSM/I F14 vs MSMR | | | |
| 50 km | < 2 h | 15 245 | 0.55 | −0.26 | 0.49 |
| | < 3 h | 97 411 | 0.52 | −0.23 | 0.47 |
| 75 km | < 2 h | 13 807 | 0.56 | −0.26 | 0.50 |
| | < 3 h | 97 750 | 0.53 | −0.23 | 0.48 |
| 150 km | < 2 h | 5065 | 0.54 | −0.26 | 0.48 |
| | < 3 h | 37 618 | 0.51 | −0.22 | 0.45 |

TABLE 6. Comparison of MSMR CLW (mg cm$^{-2}$) with TMI and SSM/I observations.

| Grid | Time | No. of points | Rmsd | Bias | Rmsd (after bias removal) |
|---|---|---|---|---|---|
| | | TMI vs MSMR | | | |
| 50 km | < 1 h | 25 923 | 13.64 | 4.42 | 12.91 |
| | < 2 h | 42 240 | 13.90 | 4.40 | 13.18 |
| | < 3 h | 57 530 | 14.29 | 4.40 | 13.59 |
| 75 km | < 1 h | 25 077 | 14.56 | 4.57 | 13.82 |
| | < 2 h | 40 894 | 14.71 | 4.54 | 13.99 |
| | < 3 h | 55 716 | 15.03 | 4.54 | 14.32 |
| 150 km | < 1 h | 10 219 | 11.89 | 5.39 | 10.60 |
| | < 2 h | 16 670 | 11.91 | 5.32 | 10.65 |
| | < 3 h | 22 616 | 12.18 | 5.39 | 10.92 |
| | | SSM/I F14 vs MSMR | | | |
| 50 km | < 2 h | 14 980 | 20.35 | 4.22 | 19.90 |
| | < 3 h | 87 916 | 19.09 | 4.51 | 18.55 |
| 75 km | < 2 h | 11 882 | 21.25 | 6.04 | 20.37 |
| | < 3 h | 76 868 | 20.02 | 6.04 | 19.08 |
| 150 km | < 2 h | 4408 | 18.98 | 6.64 | 17.78 |
| | < 3 h | 29 620 | 18.85 | 6.90 | 17.55 |

TABLE 7. Rmsd between MSMR and NOAA AVHRR SST for Jul 1999.

| Latitude belt | No. of points | Rmsd (°C) | Bias (°C) | Rmsd (°C) (after bias removal) |
|---|---|---|---|---|
| 60°–50°S | 855 | 2.327 | 1.01 | 2.09 |
| 50°–40°S | 833 | 1.55 | −0.90 | 1.27 |
| 40°–30°S | 738 | 2.51 | −2.20 | 1.20 |
| 30°–20°S | 645 | 2.14 | −1.96 | 0.87 |
| 20°–10°S | 611 | 1.83 | −1.45 | 1.11 |
| 10°S–0° | 564 | 1.29 | −0.73 | 1.07 |
| 0–10°N | 622 | 0.78 | 0.24 | 0.75 |
| 10°–20°N | 532 | 1.25 | 0.58 | 1.11 |
| 20°–30°N | 457 | 1.43 | 0.75 | 1.22 |
| 30°–40°N | 403 | 1.62 | 1.00 | 1.29 |
| 40°–50°N | 332 | 2.90 | 2.35 | 1.70 |
| 50°–60°N | 244 | 2.95 | 2.95 | 1.79 |
| Average | | 1.88 | | 1.29 |

which is better than that for MSMR. A similar order of accuracy (0.36 g cm$^{-2}$) for WV was found by Liu et al. (1992) while comparing SSM/I values with radiosonde observations at 77 stations distributed over global oceans. Alishouse (1990) compared the SSM/I WV over the range of 0–8 gm cm$^{-2}$ and found an rms error of 2 gm cm$^{-2}$.

Ali et al. (2000) also compared the MSMR-derived WS and SST with Pacific Ocean data buoy observations on a weekly basis for the same period. Since the number of in situ observations was large for this region, WS for two ranges, 0–5 and 5–10 m s$^{-1}$ were validated besides for the entire range of 0–10 m s$^{-1}$ (WS from the data buoy was not more than 10 m s$^{-1}$ even on single day). The rmsd for the entire range of 0–10 m s$^{-1}$ is 1.78 m s$^{-1}$, while it reduced to 1.52 m s$^{-1}$ for the 5–10 m s$^{-1}$ range. However, there is a marginal increase in the rmsd (1.85 m s$^{-1}$) when the 0–5 m s$^{-1}$ range is considered. This implies that MSMR wind magnitudes are better for moderate wind conditions. Meissner et al. (2001) compared the 10 yr of SSM/I WS with global analysis and found an rms error of 2.1 m s$^{-1}$ when compared with European Centre for Medium-Range Weather Forecasts analysis and 2.4 m s$^{-1}$ with National Centers for Environmental Prediction/National Center for Atmospheric Research reanalysis. The comparison with data buoy measurements revealed an rms error of 1.4 m s$^{-1}$ (Mears et al. 2001). Though the overall accuracy of the WS from MSMR is in accordance with the SSM/I (Goodberlet et al. 1990; Mears et al. 2001) and the National Aeronautics and Space Administration (NASA) scatterometer (NSCAT, Dickinson et al. 2001), a problem seems to be present in the wind magnitudes from MSMR, as discussed in section 6.

Varma et al. (2000) collocated MSMR observations with SSM/I (within 2 and 3 h of observations) and TMI (within 1, 2, and 3 h of observations) and compared in

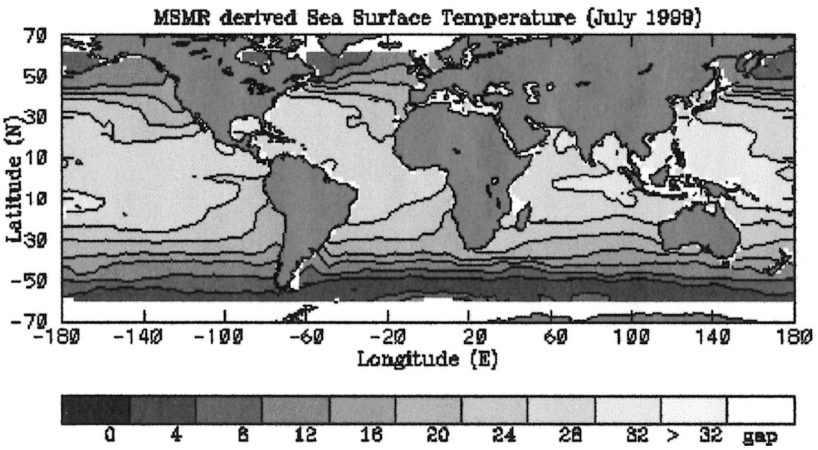


FIG. 1. Monthly averaged MSMR SST (°C) for Jul 1999.

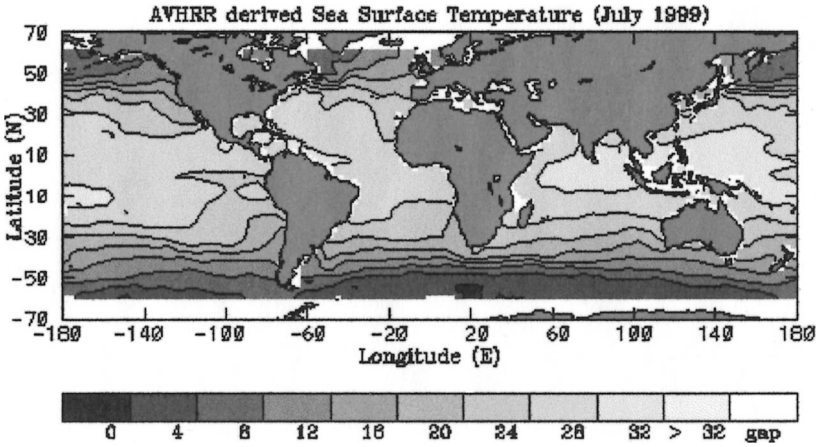


FIG. 2. Monthly averaged AVHRR SST (°C) for Jul 1999.

detail the values of WS, WV, and CLW. Their results were summarized by Ali et al. (2000) and the tables used by them are reproduced here as Tables 4, 5, and 6. A detailed comparison is given in Varma et al. (2000). In all the cases MSMR compared well with TMI compared to SSM/I.

Ali et al. (2000) found an rmsd of 1.09 K in MSMR SST when compared with in situ observations over the Indian Ocean. Weekly averaged MSMR SST was also compared with the National Oceanic and Atmospheric Administration (NOAA) Advanced Very High Resolution Radiometer (AVHRR) for different regions of the globe (Table 7). Bias is negative between 50°S and 0° in each 10° belt. Rmsd is largest in the belt 50°–60°S. This is due to possible ice contamination. In all the other belts, rmsd is less than 1.8°C. In the belt 50°–60°N, a very high positive bias (2.95°C) is observed, which suggests that MSMR is overestimating SST over this region.

## 5. Analysis

In the present study, WS of grid I and WV and CLW of grid III were used because the accuracies of these parameters for these grids are better than the other resolutions. The biases were applied to the GPD for the 70-day (15 June–23 August 1999) period during which extensive validation was carried out. All the data were binned into 2° latitude × 2° longitude grids for July 1999 using the inverse square interpolation technique with a search radius of 3°. To study the latitudinal distribution, each parameter was zonally averaged over the 70-day period over the entire longitude belt at each 2° latitude interval. In addition, correlations between each of these parameters were also obtained.

## 6. Results

The monthly averaged MSMR SST distribution for July 1999 is shown in Fig. 1. All the large-scale features

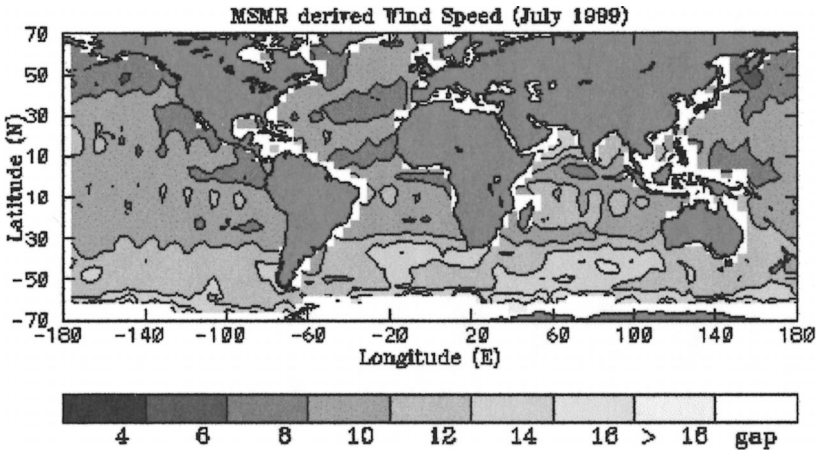


FIG. 3. Monthly averaged MSMR sea surface wind (m $s^{-1}$) for Jul 1999.

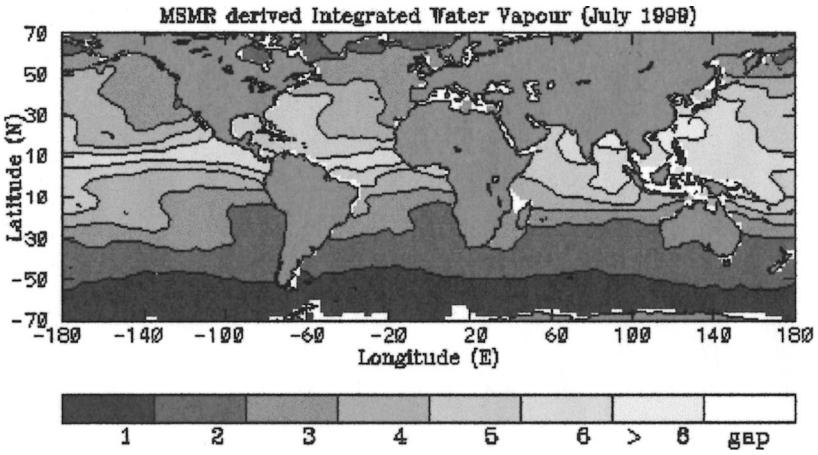


FIG. 4. Monthly averaged MSMR LWC (g cm$^{-2}$) for Jul 1999.

are well captured by MSMR SST distribution. SST distribution for July agrees within $\pm 1^{\circ}$C over a large portion (62%) of the ocean when compared with NOAA AVHRR (Fig. 2). The global temperature distribution is in conformation with the circulation of the major current systems. For example, uniform temperatures of the western Pacific, large temperature gradients toward the northwestern Pacific associated with Kuroshio Current, and cooler temperatures along the Peru coast, etc., are well reproduced. The cold tongue toward the eastern Pacific, due to the upwelling, is well defined in MSMR SST distribution. The warm equatorial tongue of the Pacific and eastern equatorial Indian Ocean are also observed in SST distribution. The latitudinal extent of warming in the western Pacific is as expected. Cooler waters in the Southern Hemisphere are due to the southern winter.

Large-scale dominant features are also present in the monthly averaged MSMR WS (Fig. 3). Though the wind speed can vary significantly within any given period, the dominant features can be inferred clearly. Strong winds associated with easterlies are more marked in the Southern Hemisphere than in the Northern Hemisphere. High winds at 50°S are prominent. This subpolar storm is present throughout the year, as observed by Grassl et al. (2000) using SSM/I wind speed observations. In the Indian Ocean, WS greater than 15 m s$^{-1}$ was observed toward the northwest Arabian Sea, which is due to the Somali jet associated with the southwest monsoon. The equatorial region of low wind speed, due to doldrums (well marked in Fig. 3), was also observed in the atlas prepared by Halpern et al. (2000). MSMR-derived WS seems to have a problem due to which elliptical patches of high winds are present (the cause for these patches is still under investigation by the concerned groups, and no consensus has been arrived at). However, since the difference between the high values in the patches and the adjoining locations is $\sim$2 m s$^{-1}$ (which is the accuracy of the observations), the large-scale features observed in this analysis would not have been affected significantly. However, this is the limitation of this parameter from MSMR.

An examination of the monthly average maps of WV and CLW content (Figs. 4 and 5, respectively) reveal

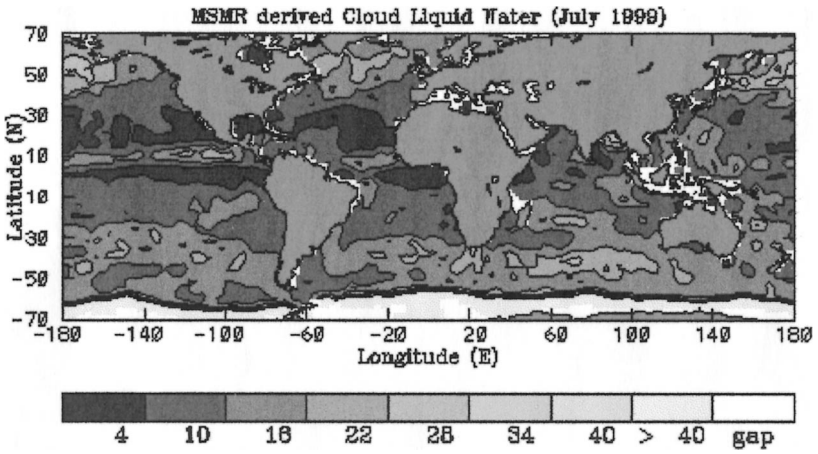


FIG. 5. Monthly averaged MSMR CLW (mg cm$^{-2}$) for July 1999.

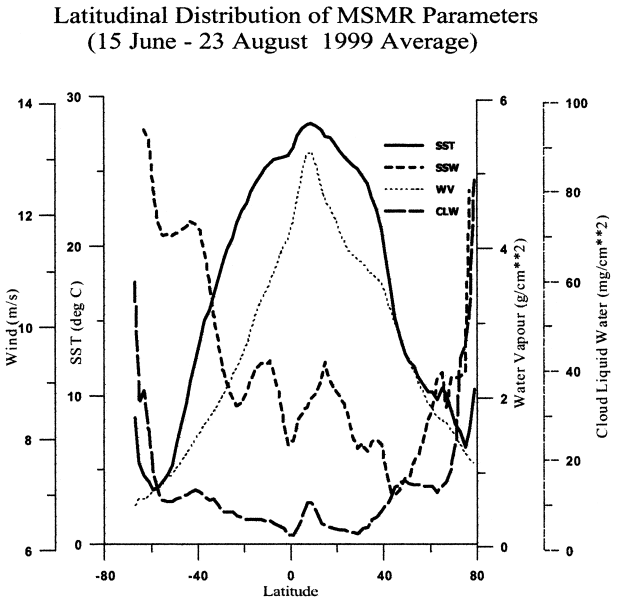


FIG. 6. Zonally averaged MSMR SST, WS, LWC, and CLW for the period 15 Jun–23 Aug 1999.

several interesting features. In subtropical areas, a certain break of zonality in the WV distribution is observed over cool and warm ocean current in the North and South Pacific. The maximum of the WV distribution elongated in the zonal direction over the equatorial region north of the equator is apparently associated with the intertropical convergence zone (ITCZ). Similar features are also observed in the earlier study carried out by Ferraro et al. (1996) using SSM/I measurements (Chang et al. 1984; Staelin et al. 1976; Grody et al. 1980; Prabhakara et al. 1982). A marked contrast in the amount of WV over the eastern and western parts of the ocean (Fig. 3) is characterized by a large amount of WV toward the west and a relatively dry zone (less WV) toward the eastern part. The SST from MSMR (Fig. 1) also brought out similar features (low and high SST corresponding to low and high WV content, respectively) in this region. Bjerknes (1969) had suggested that the strong SST gradient observed in the east–west direction over the equatorial Pacific is a triggering mechanism for a zonally oriented Walker circulation resulting in a strong jet stream in the midlatitudes. The dry zone in the eastern Pacific coincides with the sinking branch of the Walker circulation where cooler SSTs are observed. In contrast, the wet zone over the western equatorial Pacific near Indonesia–Borneo corresponds to the rising branch of the Walker circulation. The large amount of WV found in the region where high SSTs are observed may be attributed to the intense transport of WV from the ocean to the atmosphere that is associated with the prevailing convective and turbulent diffusion taking place in the area. Most of the characteristics described above were also revealed in the earlier studies using satellite data as well as conventional measurements (Chang et al. 1984; Grody et al. 1980; Prabhakara et al. 1982; Viswanadham et al. 1980). This type of large-scale feature has been observed earlier, using SMMR on board *Seasat* (Njoku and Swanson 1983).

TABLE 8. Correlation between MSMR 70-day averaged parameters.

| | SST | WS | WV |
|---|---|---|---|
| WS | −0.57 | — | — |
| WV | 0.90 | −0.58 | — |
| CLW | −0.53 | 0.46 | −0.40 |

Figure 6 represents all the large-scale meridional features of these parameters. Tropical high in SST and WV, low in WS and CLW, etc., are similar to those observed by Njoku and Swanson (1983) using 90-day (11 July–10 October 1978) averaged parameters obtained form *Seasat* SMMR. These features were also captured by Njoku and Swanson (1983). SST and WV are high in the tropical region with lower SST near the equator, caused by the equatorial upwelling. The shift of equatorial maxima around 5°N, as a result of the Northern Hemisphere summer, is also clearly brought out by this zonal distribution. From 60°S to 60°N, WV almost follows the SST pattern, showing a good correlation between these two parameters, as is evident from Table 8.

Correlation coefficients between each parameter are given in Table 8. The high positive correlation between SST and WV is well justified, as the increase in surface temperature results in increased evaporation. Wind speed decreases the SST through evaporation and, hence, they are anticorrelated. Since SST depends upon other factors like insolation and internal mixed layer dynamics, the correlation coefficient between SST and wind speed is not very significant.

## 7. Conclusions

MSMR could capture the large-scale oceanographic and meteorological features. A positive east–west gradient in Pacific Ocean SST is well reflected in the MSMR-derived SST patterns. A similar feature is also observed in the NOAA AVHRR–derived SST. Other dominant features observed in the SST patterns are uniform temperatures of the western Pacific, large temperature gradients toward the northwestern Pacific associated with the Kuroshio Current, and cooler temperatures along the Peru coast, etc. The Somali region experienced wind speed as high as 15 m $s^{-1}$ associated with the Somali jet. In spite of the problem in wind speed, large-scale features like low wind speed in the equatorial regions and high winds of subpolar storms are clearly identified. A high amount of WV has been observed over the ITCZ. The latitudinal distribution of SST and WV show large values in the tropical region with a small low in SST near the equator due to the equatorial upwelling.

*Acknowledgments.* Several teams and groups were responsible in bringing the MSMR raw data to the GPD level. The authors acknowledge the afforts of all those involved in this process. They are also thankful to Gohil et al. (2000) and Varma et al. (2000) for allowing them to use some of their results. Constructive criticism from the three referees helped the authors to improve the paper. They are grateful to them. NOAA AVHRR digital data have been downloaded from the NOAA ftp site.

## REFERENCES

Ali, M. M., and Coauthors, 2000: Validation of multifrequency scanning microwave radiometer geophysical parameter data products. Preprints, *Fifth Pacific Ocean Remote Sensing Conf. (PORSEC)*, Goa, India, National Institute of Oceanography, 182–191.

Alishouse, J. C., S. A. Synder, J. Vongsathorn, and R. R. Ferraro, 1990: Determination of oceanic total water from the SSM/I. *IEEE Trans. Geosci. Remote Sens.,* **28,** 811–816.

Bernstein, R. L., 1982: SST mapping with the Seasat microwave radiometer. *J. Geophys. Res.,* **87,** 7865–7872.

——, and J. H. Morris, 1983: Tropical and mid-latitude North Pacific sea surface temperature variability from the Seasat SMMR. *J. Geophys. Res.,* **88,** 1877–1891.

Bjerknes, J., 1969: Atmospheric teleconnections from the equatorial Pacific. *Mon. Wea. Rev.,* **97,** 163–172.

Chang, H. D., P. H. Hwang, T. T. Wilheit, A. T. C. Chang, D. H. Staelin, and P. W. Rosekranz, 1984: Monthly distribution of precipitable water from the Nimbus-7 SMMR data. *J. Geophys. Res.,* **89,** 5328–5334.

Chelton, D. B., K. J. Hussey, and M. E. Parke, 1981: Global satellite measurements of water vapour, wind speed and wave height. *Nature,* **294,** 529–532.

Dickinson, S., K. A. Kelly, M. J. Caruso, and M. J. McPhaden, 2001: Comparison between the TAO buoy and NASA scatterometer wind vectors. *J. Atmos. Oceanic Technol.,* **18,** 799–806.

Ferraro, R. R., F. Weng, N. C. Grody, and A. Basist, 1996: An eight-year (1987–1994) time series of rainfall, clouds, water vapor, snow cover and sea ice derived from SSM/I measurements. *Bull. Amer. Meteor. Soc.,* **77,** 891–905.

Gohil, B. S., A. K. Mathur, and A. K. Varma, 2000: Geophysical parameter retrieval over global oceans from IRS-P4/MSMR. Preprints, *Fifth Pacific Ocean Remote Sensing Conf. (PORSEC),* Goa, India, National Institute of Oceanography, 207–211.

Goodberlet, M. A., C. T. Swift, and J. C. Wilkerson, 1990. Ocean surface wind speed measurements of the Special Sensor Microwave/Imager (SSM/I). *IEEE Trans. Geosci. Remote Sens.,* **28,** 823–828.

Grassl, H., V. Jost, J. Schulz, M. R. Ramesh Kumar, P. Bauer, and P. Schluessel, 2000: The Hamburg Ocean–Atmosphere Parameters and fluxes from satellite data (HOAPS): A climatological atlas of satellite-derived air–sea interaction parameters over the world oceans. Max-Planck-Institut für Meteorologie Rep. 312, 130 plates.

Grody, N., A. Gruber, and W. Shen, 1980: Atmospheric water content over the tropical Pacific derived from the Nimbus-6 scanning microwave spectrometer. *J. Appl. Meteor.,* **19,** 986–996.

Halpern, D., O. B. Brown, G. C. Feldman, M. H. Freilich, and F. J. Wentz, 2000: An atlas of monthly mean distributions of SSMI surface wind speed, AVHRR SST, TMI SST, AMI surface wind velocity, SeaWiFS chlorophyll-a, and TOPEX/POSEIDON sea surface topography during 1998. JPL Publication 00-08, NASA, 111 pp.

Hollinger, J. P., 1971: Passive microwave measurements of sea surface roughness. *IEEE Trans. Geosci. Electron.,* **GE-9,** 165–169.

Liebe, H. J., 1985: An updated model for millimetre wave propagation in moist air. *Radio Sci.,* **20,** 1069–1089.

Liu, W. T., W. Tang, and F. J. Wentz, 1992: Precipitable water and surface humidity over global oceans from Special Sensor Microwave Imager and European Centre for Medium Range Weather Forecasts. *J. Geophys. Res.,* **97,** 2251–2264.

Mears, C. A., D. K. Smith, and F. J. Wentz, 2001: Comparison of Special Sensor Microwave Imager and buoy-measured wind speeds from 1987 to 1997. *J. Geophys. Res.,* **106,** 11 719–11 729.

Meissner, T., D. Smith, and F. Wentz, 2001: A 10 year intercomparison between collocated Special Sensor Microwave Imager oceanic surface wind speed retrievals and global analyses. *J. Geophys. Res.,* **106,** 11 731–11 742.

Njoku, E. G., and L. Swanson, 1983: Global measurements of sea surface temperature, wind speed and atmospheric water content from satellite microwave radiometry. *Mon. Wea. Rev.,* **111,** 1977–1987.

Prabhakara, C., H. D. Chang, and A. T. C. Chang, 1982: Remote sensing of precipitable water over the oceans from Nimbus-7 microwave measurements. *J. Appl. Meteor.,* **21,** 59–68.

Staelin, D., K. Kunzi, R. Pethyjohn, R. Poon, R. Wilcox, and J. Waters, 1976: Remote sensing of atmospheric water vapor and liquid water with the Nimbus-5 microwave spectrometer. *J. Appl. Meteor.,* **15,** 1204–1214.

Starr, V. P., and R. M. White, 1955: Direct measurement of the hemispheric poleward flux of water vapour. *J. Mar. Res.,* **14,** 217–225.

——, and J. P. Peixoto, 1958: On the global balance of water vapour and the hydrology of deserts. *Tellus,* **10,** 189–194.

——, ——, and R. G. McKean, 1969: Pole-to-pole moisture conditions for the IGY. *Pure Appl. Geophys.,* **75,** 300–331.

Stogryn, A., 1972: The emissivity of sea foam at microwave frequencies. *J. Geophys. Res.,* **77,** 1658–1666.

Varma, A. K., R. M. Gairola, A. K. Mathur, B. S. Gohil, and V. K. Agarwal, 2000: Intercomparison of IRS-P4-MSMR derived geophysical products with DMSP-SSM/I, TRMM-TMI and NOAA-AVHRR finished products. Preprints, *Fifth Pacific Ocean Remote Sensing Conf. (PORSEC),* Goa, India, National Institute of Oceanography, 192–196.

Viswanadham, Y., J. M. Rao, and G. S. S. Nunes, 1980: Some studies on moisture conditions in the Southern Hemisphere. *Tellus,* **32,** 131–142.

Wentz, F. J., C. Gentermann, D. Smith, and D. Chelton, 2000: Satellite measurements of sea surface temperature through clouds. *Science,* **288,** 847–850.

Wilheit, T. T., 1979: A model for the microwave emissivity of the ocean's surface as a function of wind speed. *IEEE Trans. Geosci. Electron.,* **4,** 244–249.

Yang, S., and E. A. Smith, 1999: Moisture budget analysis of TOGA COARE area using SSM/I retrieved latent heating and large-scale Q2 estimates. *J. Atmos. Oceanic Technol.,* **16,** 633–655.